

Quantum simulation of multiple-exciton generation in a nanocrystal by a single photon

Wayne M. Witzel,^{1,2} Andrew Shabaev,³ and C. Stephen Hellberg¹, Verne L. Jacobs¹, and Alexander L. Efros¹

¹*Naval Research Laboratory, Washington DC 20375 USA*

²*Sandia National Laboratories, NM 87185 USA*

³*George Mason University, VA 22030 USA*

(Dated: June 16, 2018, MEG-shortResubmAE.tex, printing time = 13:15)

We have shown theoretically that efficient multiple exciton generation (MEG) by a single photon can be observed in small nanocrystals (NCs). Our quantum simulations that include hundreds of thousands of exciton and multi-exciton states demonstrate that the complex time-dependent dynamics of these states in a closed electronic system yields a saturated MEG effect on a picosecond timescale. Including phonon relaxation confirms that efficient MEG requires the exciton–biexciton coupling time to be faster than exciton relaxation time.

PACS numbers:

Solar light would be an important source of clean and renewable energy if the efficiency of inexpensive solar cells could be increased. Increased efficiency can be achieved through carrier multiplication: Photo-generated carriers, whose excess energy is greater than the energy gap, can create secondary electron-hole pairs via impact ionization of the filled band. Through this process, two (or more) electron-hole pairs are collected from each photon instead of just one. This process is very inefficient in bulk semiconductors, where impact ionization has a very low probability and carrier thermalization, which always competes with impact ionization, is much faster.

As first suggested by Nozik, impact ionization may effectively compete with cooling in NCs, due to the enhanced rate of inverse Auger processes for carrier multiplication and the “phonon bottleneck” suppression of carrier relaxation, leading to efficient MEG [1]. Soon after this publication, Schaller and Klimov [2] observed ultra-efficient MEG by a single photon in PbSe NCs, using band-edge transient absorption measurements. Later, efficient MEG was observed by many groups using different techniques in NCs of many semiconductors: PbSe [3–6], PbS [3, 7], Si [8], CdSe [9–11], InAs [12, 13], and in carbon nanotubes [15]. At the same time, some groups were not able to observe MEG in CdSe [16] and InAs [14, 17] NCs and found that the efficiency of MEG measured in PbSe NCs [6] was appreciably smaller than that reported earlier. The diverse experimental data on the MEG efficiency are now converging to more modest values for PbS and PbSe NCs [18], but MEG in NCs has been shown to be significantly more efficient than impact ionization in bulk semiconductors [19, 20].

Previous attempts at a theoretical understanding of the enhanced MEG provide only estimations of the MEG efficiency observed in NCs [3, 21–26]. A self-consistent theory of this phenomena requires a currently non-existent theoretical description of both the relaxation mechanisms for and couplings between the highly excited exciton and multi-exciton states in NCs [24]. To explain the high efficiency of MEG in NCs, the coherent

superposition model, based on the strong quasi-resonant coupling between exciton and multi-exciton states in a NC, was proposed [3, 24]. Non-coherent models for efficient MEG in NCs [21–23, 26] are based on the important observation that the density of biexciton states is significantly larger than the density of exciton states at the same energy [21], and the density of trion states is particularly important for efficient MEG [25]. The calculations of MEG efficiency in all of these non-coherent models are based on Fermi’s Golden Rule, which requires the final biexciton state to decay much faster than the rate of the exciton–biexciton transition, an assumption that has not been justified either experimentally or theoretically.

In this letter we unify both approaches and consider a single-photon excitation coherently coupled with multi-exciton-states in a NC within a full quantum-state evolution approach. The time-dependent dynamics of our modeled systems is described using a large multiple-configuration basis representation of the many-electron Hamiltonian, including energy non-conserving exciton and biexciton decay channels. The calculations show that even in a closed, energy-conserving electronic system, the excitation becomes predominantly multi-excitonic on a picosecond time scale. The initial single-photon excitation is dispersed into the dense multi-exciton state space of the NC.

We consider a single-photon excitation of a spherical PbSe NC, where efficient MEG has been reported [2–6]. The energy spectrum of electrons and holes at the band edges of four equivalent L valleys of bulk PbSe is described by a four band $\mathbf{k} \cdot \mathbf{p}$ model [27]. In PbSe NCs each electron, $n^e L_m^j$, and hole, $n^h L_m^j$, state within the four-band effective-mass model [28], is characterized by the spatial angular momentum $L = 0(S), 1(P), 2(D), 3(F), \dots$, the total angular momentum $j = L \pm 1/2$, which is the sum of the angular momentum and the spin, the projection of the total momentum $m = \pm 1/2, \pm 3/2, \dots \pm j$, and the spatial inversion parity π . The energy levels of the same symmetry were calculated using energy band parameters from Ref. 3 and

labeled by a level number, $n^{e,h}$. The four envelope components, $F_i(\mathbf{r})$, ($i = 1, 2, 3, 4$) of the corresponding single-particle wavefunctions can be expressed in the form:

$$F_i(\mathbf{r}) = C_i^{L,m,\pi} f_{\tilde{L}_i^\pi}^n(r) Y_{\tilde{L}_i^\pi}^{\tilde{m}_i^\pi}(\theta, \phi), \quad (1)$$

where $C_i^{L,m,\pi}$ are constants, $f_l^n(r)$ are specific radial functions expressed in terms of the spherical Bessel functions, $\tilde{L}_i^\pi = L$ or $L + 1$ and $\tilde{m}_i^\pi = m \pm 1/2$ (depending upon the values of i and π), and $Y_{\tilde{L}_i^\pi}^{\tilde{m}_i^\pi}(\theta, \phi)$ are the spherical harmonics.

The Coulomb coupling of an electron or hole with multi-electron-hole excitations at the same energy, which are disallowed in the bulk due to momentum conservation, plays an important role for MEG in NCs [24]. We generate a Hamiltonian matrix in the basis of many-electron states that are Slater determinants of single-particle eigenstates. A many-electron state in this approach is a set of occupied conduction states (electrons) and unoccupied valence states (holes) with an arbitrary but consistent sign convention for the Slater-determinant permutations. We include many-electron basis states up to some chosen energy cut-off that we adjust until the results converge (see Fig. 1). We modeled the Coulomb interaction using effective dielectric constants for the NC, κ_s , and surrounding media, κ_g , leading to the direct Coulomb interaction between electrons at positions \mathbf{r} and \mathbf{r}' in the NC, $V_C(\mathbf{r}, \mathbf{r}') = e^2/(\kappa_s |\mathbf{r} - \mathbf{r}'|)$, and the surface mediated Coulomb potential [29], $V_S(\mathbf{r}, \mathbf{r}') = e^2 a / (\tilde{\kappa} r' |\mathbf{r} - a^2 \mathbf{r}' / r'^2|)$, where a is the NC radius and $\tilde{\kappa}^{-1} = 2(\kappa_s - \kappa_g) / \kappa_s(\kappa_s + 2\kappa_g)$. We also account for the electron and hole interaction with their image potentials described by $V_e(r) = V_h(r) = 0.5V_s(\mathbf{r}, \mathbf{r})$.

The diagonal elements of this Hamiltonian matrix are taken to be sums of the single-particle-state energies (including image potentials) and the Coulomb interactions among electrons and holes (including the exchange interactions from Fermi permutations). Off-diagonal elements couple basis states that differ in either two or four sets of single-state occupations via the Coulomb interaction.

Because the single-particle states in the spherical NCs are represented in terms of spherical harmonics, it is most efficient to express the Coulomb potentials $V_C(\mathbf{r}, \mathbf{r}')$ and $V_S(\mathbf{r}, \mathbf{r}')$ in terms of spherical harmonics [29]:

$$V_C(\mathbf{r}, \mathbf{r}') = \frac{4\pi e^2}{\kappa_s} \sum_{l=0}^{\infty} \frac{1}{2l+1} \frac{r_{<}^l}{r_{>}^{l+1}} \Upsilon_l(\theta, \phi, \theta', \phi'), \quad (2)$$

$$V_S(\mathbf{r}, \mathbf{r}') = \frac{4\pi e^2}{a\tilde{\kappa}} \sum_{l=0}^{\infty} \frac{1}{2l+1} \left(\frac{rr'}{a^2} \right)^l \Upsilon_l(\theta, \phi, \theta', \phi'),$$

where $\Upsilon_l(\theta, \phi, \theta', \phi') = \sum_m Y_{lm}^*(\theta', \phi') Y_{lm}(\theta, \phi)$, \mathbf{r} and \mathbf{r}' are represented by $\{r, \theta, \phi\}$ and $\{r', \theta', \phi'\}$ in spherical coordinates, $r_{>} = \max(r, r')$, and $r_{<} = \min(r, r')$. Using these expressions, we have performed integrations

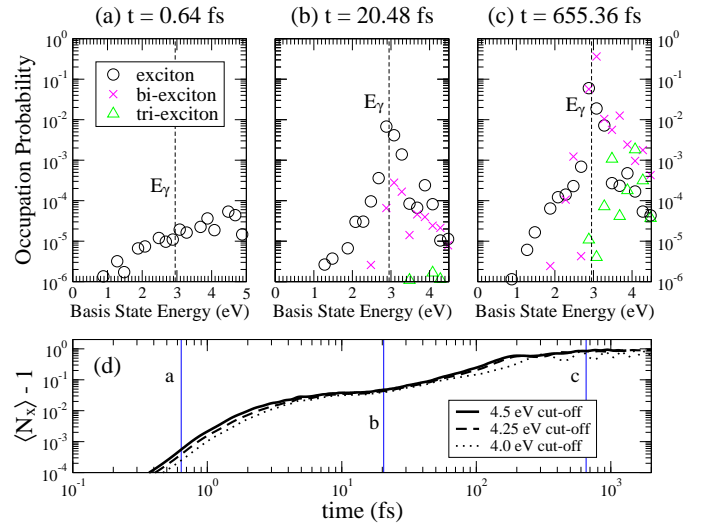


FIG. 1: Time dependent evolution of the $2^e P_{1/2}^{1/2} - 2^h P_{1/2}^{1/2}$ excitation created in the 2 nm radius PbSe NC with $\kappa_s = \kappa_g = 5$ by a single $E_\gamma = 2.95$ eV photon calculated for the closed-system. The upper panels (a,b,c) show the occupation probabilities of exciton, bi-exciton and tri-exciton states over 0.2 eV wide energy bins at three times. Panel (d) demonstrates convergence of the time dependence of the relative number of excitons $\langle N_x(t) \rangle - 1$, defined in Eq. (3), achieved by adjusting the energy cut-off. The vertical lines a, b and c show the times corresponding to the three upper panels.

involving the angular components analytically by exploiting the orthonormality of the spherical harmonics.

The remaining radial parts of the integrals of the Coulomb matrix elements take the form $\int dr \int dr' f_i^m(r) f_j^n(r) f_k^o(r') f_l^p(r') [(r_{<})^l / (r_{>})^{l+1}]$, or $\int dr \int dr' f_i^m(r) f_j^n(r) f_k^o(r') f_l^p(r') (1/rr')^{l+1}$, where $f_i^m(r)$ are the radial functions defined in Eq. (1) for the envelope eigenfunctions that are expressed via spherical Bessel functions. In our computational implementation, we approximate these Bessel function integrals as needed by Monte-Carlo sampling and store the result for future reference. A sufficient number of samples was taken to reach a specified level of precision for the matrix elements [30]. At a 4.8 eV cut-off used to simulate the 2 nm radius NCs, the basis contains hundreds of thousands of many-electron states, and the Hamiltonian matrix contains tens of millions of non-zero elements.

To incorporate the interaction involving a single photon, we adopt the standard effective-mass approximations that the wavelength of the photon is much larger than the NC size and that the contributions of the Bloch functions are dominant in the integral over the electron momentum operator [28]. In the PbSe NCs with symmetric conduction and valence bands, we assume that the photons are coupled exclusively to symmetric electron-hole pairs, in which both the electron and the hole have the same quantum numbers. As a result the NC-photon

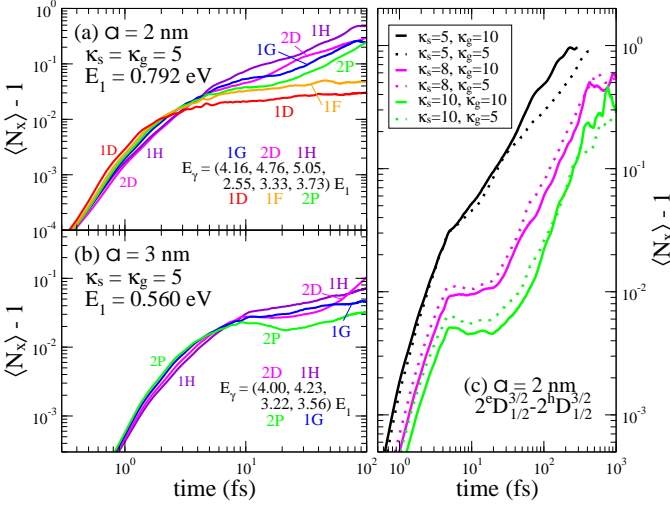


FIG. 2: Time dependent evolution of the relative number of excitons $\langle N_x(t) \rangle$, defined in Eq. (3), created by a single-photon excitation of various optical transitions in PbSe NCs with radii 2 nm (a) and 3 nm (b) calculated for the closed-system with $\kappa_s = \kappa_g = 5$. The optical transitions $2^e P_{1/2}^{1/2} - 2^h P_{1/2}^{1/2}$, $1^e D_{1/2}^{3/2} - 1^h D_{1/2}^{3/2}$, $1^e F_{1/2}^{5/2} - 1^h F_{1/2}^{5/2}$, $2^e P_{1/2}^{1/2} - 2^h P_{1/2}^{1/2}$, $1^e G_{1/2}^{7/2} - 1^h G_{1/2}^{7/2}$, $2^e D_{1/2}^{3/2} - 2^h D_{1/2}^{3/2}$, $1^e H_{1/2}^{9/2} - 1^h H_{1/2}^{9/2}$, are abbreviated 1D, 1F, 2P, 1G, 2D, and 1H respectively with energies shown in units of the effective energy gap $E_1(a)$. Panel (c) shows the evolution of $\langle N_x(t) \rangle$ created by a single-photon excitation of the $2^e D_{1/2}^{3/2} - 2^h D_{1/2}^{3/2}$ transition in a 2 nm radius PbSe NC calculated for various combinations of the dielectric constants of the nanocrystal κ_s and the surrounding media κ_g .

interaction is characterized by a single parameter corresponding to the coupling energy. Furthermore, our results are obtained in the weak-coupling single-photon limit, where the actual coupling strength is irrelevant provided that it is sufficiently small.

Let us begin from a study of the closed system evolution. Starting from an initial single-photon-state, electronic states are excited and evolve through Coulombic interactions. In each simulated experiment, the photon energy was chosen to match one of the optically active exciton states, because the NC absorption spectra are not affected by the coupling between excitons and multi-exciton states [24]. We evolve the initial state using the Schrödinger equation, $d|\Psi(t)\rangle/dt = -i\hat{H}|\Psi(t)\rangle/\hbar$, where \hat{H} is our Hamiltonian that includes all interactions considered above. Using a differential equation solver [31] for integration, we adjusted the precision until we obtained convergent results.

Figure 1 shows the time-dependent evolution of the $2^e P_{1/2}^{1/2} - 2^h P_{1/2}^{1/2}$ excitation created by a single photon calculated for our closed-system description. The upper panels (a,b,c) show the occupation probabilities $\| \langle k|\Psi(t) \rangle \|^2$ of exciton, bi-exciton and tri-exciton states

created from the photon at three different snapshots in time. The initially created excitons are replaced by the biexcitons in approximately 0.3 ps. Formation of triexcitons at the excitation energy considered, $2.95eV \sim 3.73E_1(a)$ where $E_1(a)$ is the effective energy gap, is limited, however, in our single valley model, which allows only two electron-hole pairs to occupy the ground state. Figure 1(d) shows the time dependence of the expectation value for the relative number of excitons:

$$\langle N_x(t) \rangle = \sum_{n=1}^3 n \sum_{k \in \mathcal{K}_n} \| \langle k|\Psi(t) \rangle \|^2 / \sum_{l>0} \| \langle l|\Psi(t) \rangle \|^2, \quad (3)$$

where \mathcal{K}_n is the set of n -exciton basis states. In the small NC with small dielectric constant considered in Fig. 1, the strong Coulomb coupling rapidly creates a bi-exciton with 90% probability.

We also investigate how $\langle N_x(t) \rangle$ depends on the excitation energy and the Coulomb coupling, which in our model is controlled by the NC size and dielectric constants. Figure 2(a) compares the formation of multi-excitons from a single photon excitation of different optical transitions in the 2 nm radius NC. The $2^e P_{1/2}^{1/2} - 2^h P_{1/2}^{1/2}$ transition appears to provide a threshold for efficient MEG generation in PbSe NCs: while lower transitions saturate at around 10 fs to a low probability of biexciton generation, the multi-exciton number continues to increase when the threshold is reached. This is because the $2^e P$ and $2^h P$ states are the first that can be strongly coupled with trions of the same energy [24]. Increasing the NC size [Fig. 2(b)] and the dielectric constant [Fig. 2(c)] significantly increases the time of MEG generation. Both effects are the direct result of the reduced Coulomb coupling.

Note that the evolution of $\langle N_x(t) \rangle$ does not show strong oscillations when MEG is efficient, even for a closed system. Oscillations are seen only in the striking cross-over behavior in Fig. 2 (a) and (b), which is the result of the different coupling strengths and detunings between the multi-exciton states and the exciton created by the resonant light. The coherent oscillations connecting the exciton and biexciton states are suppressed due to the large number of interacting biexciton states. Once the excitation evolves into the dense multi-exciton state space, it does not appreciably revive.

Phonon-assisted assisted relaxation of carriers, which was not considered above, can strongly affect the MEG efficiency [24]. The evolution of $\langle N_x(t) \rangle$, including phonon decay, is described by

$$\frac{d}{dt}|\Psi\rangle = -\frac{i}{\hbar}\hat{H}|\Psi\rangle - \sum_n \sum_{k \in \mathcal{K}_n} \frac{1}{2\tau_n} \langle k|\Psi\rangle |k\rangle, \quad (4)$$

where τ_n is the relaxation time of the n -exciton state that for simplicity is assumed to depend only on n . As states decay, they are removed from the Hilbert space

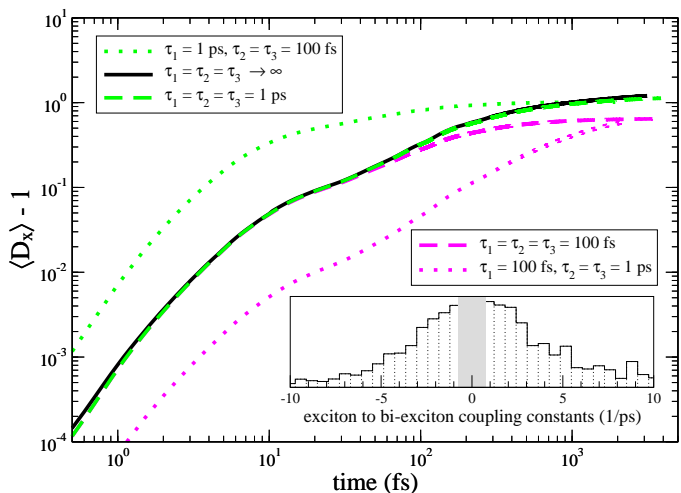


FIG. 3: Evolution of the average number of decayed-to-the-ground-state excitons $\langle D_x(t) \rangle$ created by a single-photon excitation of the $1^e H_{1/2}^{9/2} - 1^h H_{1/2}^{9/2}$ transition of a 2 nm radius PbSe NC calculated for various combinations of thermalization times. The inset shows the distribution of inverse coupling times connecting optically active exciton states and bi-exciton states, which are equal to the interaction Hamiltonian matrix elements, divided by \hbar . The 1/ps scale in the inset allows comparison of typical coupling times to thermalization times. The gray region of the coupling strengths is unresolved at our precision and excluded from the distribution.

and populate $D_n(t)$, denoting each “ground” n -exciton state and governed by $\dot{D}_n = \sum_{k \in \mathcal{K}_n} \|\langle k | \Psi \rangle\|^2 / \tau_n$ with $D_n(0) = 0$.

To find the relative number of excitons following decay, we take the weighted average $\langle D_x \rangle = \sum_n n D_n / \sum_m D_m$. We plot this average in Fig. 3 for various τ_n lifetimes. The introduction of the long and equal relaxation times $\tau_1 = \tau_2 = \tau_3 = 1$ ps has little impact upon the time dependent evolution: the system remains almost closed. Indeed, these times are much longer than an average time of the exciton-biexciton coupling as one can see in the inset of Fig. 3. Reducing the biexciton and trion decay times to $\tau_2 = \tau_3 = 100$ fs increases the rate of MEG in agreement with Ref. [24]. It is interesting to note that the saturation value for MEG depends only upon τ_1 . If this time is shorter than the exciton-biexciton coupling time, ~ 300 fs, MEG is significantly suppressed.

Our calculations of the dynamics and efficiency of MEG, unfortunately, cannot be compared with experimental data measured in PbSe NCs because they were based on a single-valley model. The lack of a precise knowledge of inter-valley coupling does not allow us to take this effect into account. The single-valley approximation should significantly underestimate the density of multiple-exciton states. For example, in real PbSe NCs one can have eight electron-hole pairs at the ground exciton state instead of only the two ground excitons allowed

in our model. The inter-valley coupling significantly increases the density of multi-exciton states; the k -exciton state density is increased by at least a factor of 4^{2k} for PbSe with its 4 valleys. For this reason, MEG should be even more efficient in a model that includes inter-valley coupling.

In summary, our calculations unambiguously demonstrate that highly efficient MEG can be observed in small NCs. The effect is enhanced by a high density of biexciton states that are strongly coupled with optically created excitons. Fast multi-exciton thermalization accelerates the formation of multi-excitons in the ground state which should improve efficiency of extraction of electron hole pairs from NCs.

We thank Andrew Taube for important scientific advice. We acknowledge financial support from ONR. A.S. acknowledge support from NIST 70NANB7H6138 Am 001, and Center for Advanced Solar Photophysics, a DOE Energy Frontier Research Center.

Sandia National Laboratories is a multi-program laboratory operated by Sandia Corporation, a wholly owned subsidiary of Lockheed Martin Corporation, for the U.S. Department of Energy’s National Nuclear Security Administration under contract DE-AC04-94AL85000.

-
- [1] A. Nozik, *Physica E* **14**, 115 (2002).
 - [2] R. D. Schaller and V. I. Klimov, *Phys. Rev. Lett.* **92**, 186601 (2004).
 - [3] R. J. Ellingson, *et. al*, *Nano Lett.*, **5**, 865 (2005).
 - [4] M. T. Trinh, *et. al*, *Nano Lett.* **8**, 1713 (2008).
 - [5] M. Ji, *et. al*, *Nano Lett.* **9**, 1217 (2009).
 - [6] G. Nair, S. M. Geyer, L.-Y. Chang, M. G. Bawendi, *Phys. Rev. B* **78**, 125325 (2008).
 - [7] R. D. Schaller, *et. al*, *Nano Lett.* **6**, 424 (2006).
 - [8] M. C. Beard, *et. al*, *Nano Letters* **7**, 2506 (2007).
 - [9] R. D. Schaller, M. A. Petruska, V. I. Klimov, *Appl. Phys. Lett.* **87**, 253102, (2005);
 - [10] R. D. Schaller, *et. al*, *J. Phys. Chem B* **110**, 25332 (2006).
 - [11] D. Gachet, *et. al*, *Nano Letters* **10**, 164 (2010).
 - [12] R. D. Schaller, J. M. Pietryga, V. I. Klimov, *Nano Lett.* **7**, 3469 (2007).
 - [13] J. J. H. Pijpers, *et. al*, *J. Phys. Chem. C* **111**, 4146 (2007).
 - [14] J. J. H. Pijpers, *et. al*, *Phys. Chem. C* **112**, 4783 (2008).
 - [15] N. M. Gabor, *et. al*, *Science* **325**, 1367 (2009).
 - [16] G. Nair, M. G. Bawendi, *Phys. Rev. B* **76**, 081304(R) (2007).
 - [17] M. Ben-Lulu, *et. al*, *Nano Lett.* **8**, 1207 (2008).
 - [18] J. A. McGuire, *et. al*, *Accounts of Chem. Research* **41**, 1810 (2008).
 - [19] M. C. Beard, *et. al*, to be published.
 - [20] J.A. McGuire, *et. al*, *NanoLett.* DOI:10.1021/nl100177c.
 - [21] R. D. Schaller, V. M. Agranovitch, and V. I. Klimov, *Nature Physics* **1**, 189 (2005).
 - [22] G. Allan and C. Delerue, *Phys. Rev. B* **73**, 205423 (2006).
 - [23] A. Franceschetti, J. M. An and A. Zunger, *Nano Lett.* **6**, 2191 (2006).

- [24] A. Shabaev, Al. L. Efros, and A. J. Nozik, NanoLetters **6**, 2856 (2006).
- [25] E. Rabani and R. Baer, Nano Letters **8**, 4488 (2008).
- [26] A. B. Madrid, *et. al*, ACS Nano **3**, 2487 (2009).
- [27] D. J. Mitchell and R. F. Wallis, Phys. Rev. **151**, 581 (1966)
- [28] I. Kang and F. W. Wise, J. Opt. Soc. Am. B **14**, 1632 (1997).
- [29] J. D. Jackson, *Classical Electrodynamics*, 2nd ed. (Wiley, New York, 1975), Chapters 2, 3, and 4. Wiley & Sons
- [30] The level of precision was tested by repeating the calculations with a different random-number-generator seed and checking for consistency.
- [31] We use a package called CVODE written by Scott D. Cohen and Alan C. Hindmarsh at Lawrence Livermore National Laboratory and available from www.netlib.org.